Li *et al. Earth, Planets and Space* (2018) 70:44
https://doi.org/10.1186/s40623-018-0814-8

Earth, Planets and Space

FULL PAPER

Open Access

A paleomagnetic record in loess–paleosol sequences since late Pleistocene in the arid Central Asia

Guanhua Li[1,2*], Dunsheng Xia[2], Erwin Appel[3], Youjun Wang[2], Jia Jia[2] and Xiaoqiang Yang[1]

Abstract

Geomagnetic excursions during Brunhes epoch have been brought to the forefront topic in paleomagnetic study, as they provide key information about Earth's interior dynamics and could serve as another tool for stratigraphic correlation among different lithology. Loess–paleosol sequences provide good archives for decoding geomagnetic excursions. However, the detailed pattern of these excursions was not sufficiently clarified due to pedogenic influence. In this study, paleomagnetic analysis was performed in loess–paleosol sequences on the northern piedmont of the Tianshan Mountains (northwestern China). By radiocarbon and luminance dating, the loess section was chronologically constrained to mainly the last c.130 ka, a period when several distinct geomagnetic excursions were involved. The rock magnetic properties in this loess section are dominated by magnetite and maghemite in a pseudo-single-domain state. The rock magnetic properties and magnetic anisotropy indicate weakly pedogenic influence for magnetic record. The stable component of remanent magnetization derived from thermal demagnetization revealed the presence of two intervals of directional anomalies with corresponding intensity lows in the Brunhes epoch. The age control in the key layers indicates these anomalies are likely associated with the Laschamp and Blake excursions, respectively. In addition, relative paleointensity in the loess section is basically compatible with other regional and global relative paleointensity records and indicates two low-paleointensity zones, possibly corresponding to the Blake and Laschamp excursions, respectively. As a result, this study suggests that the loess section may have the potential to record short-lived excursions, which largely reflect the variation of dipole components in the global archives.

Keywords: Geomagnetic excursion, Blake excursion, Laschamp excursion, Relative paleointensity, Loess, Arid Central Asia

Introduction

Geomagnetic excursions, characterized by short-lived geomagnetic polarity swings on a brief period of several 1000 years, provide a window to intrinsic characteristics of geodynamo (e.g., Channell 2006; Roberts 2008; Singer 2014). Since the middle of the twentieth century, geomagnetic excursions were emphasized in different lithological materials during the intensified study of paleomagnetic reversals, greatly improving the knowledge of historic variation of geomagnetic field (Laj and Channell 2007). There are more than fifteen excursions that have already been reported within Brunhes epoch, and most directional excursions were basically accompanied by paleointensity lows (Valet and Meynadier 1993). With regard to the periods since last interglacial, two important excursions, Blake and Laschamp excursions, have received great attention around the world. The Blake geomagnetic excursion (BGE) has been found in different lithologies since it was introduced by Smith and Foster (1969). The BGE was regarded as one of the most apparent intensity lows in the geomagnetic dipole moment and was chronologically confined in marine isotope stage 5 ranging from about 118 to 100 ka BP by previous studies (Laj and Channell 2007; Singer 2014; Guillou et al. 2016). There are three main types of polarity variations among

*Correspondence: ligh1986@gmail.com
[1] Guangdong Provincal Key Laboratory of Geodynamics and Geohazards, School of Earth Sciences and Engineering, Sun Yat-sen University, Guangzhou 510275, China
Full list of author information is available at the end of the article

the published studies on the BGE, characterized by single (Tucholka et al. 1987), double (Denham 1976; Fang et al. 1997; Osete et al. 2012) or even ternary (Zhu et al. 1994) reversed-polarity zones. Despite hot discussions about the dating and duration of the BGE, this excursion is now accepted as a globally geomagnetic anomaly in the late Quaternary (Singer 2014). Another one known as the Laschamp geomagnetic excursion (LGE) delivered a valuable record of temporal field variability in the late Quaternary. Shortly before the report of the pioneering polarity chronology, Bonhommet and Babkine (1967) identified anomalous signals related to the LGE, based on a paleomagnetic study of lava flows in the Massif Central, France. Since then, the LGE has been observed in various sediments around the globe, characterized by directional variations and low paleointensities (e.g., Lund et al. 2005, 2017; Laj and Channell 2007; Yamazaki and Kanamatsu 2007; Cassata et al. 2008; Singer et al. 2009; Nowaczyk et al. 2012). The age of the LGE was recently determined at c.41 ka (e.g., Singer et al. 2009; Lascu et al. 2016; Lund et al. 2017).

As an important terrestrial archive, loess deposits in the Chinese Loess Plateau (CLP) also clearly contain anomalous directions related to the LGE (Zhu et al. 1999, 2006; Zhou et al. 2010; Sun et al. 2013) and BGE (Zhu et al. 1994; Zheng et al. 1995; Fang et al. 1997; Zhou et al. 2010). However, the timing and duration of the excursions recorded in the loess sections are not well determined because remanence acquisition is possibly influenced by post-depositional processes (Roberts and Winklhofer 2004; Sun et al. 2013). Moreover, lock-in depths seem to cause increasing problems toward the southeastward direction on the CLP where certain excursion is missing or poorly captured in most sections (Sun et al. 2013). Recently, with the aid of cosmogenic nuclides analysis (Zhou et al. 2010), reassessment of the BGE and LGE excursions in some of the classic sections on the CLP revealed a record of geomagnetic intensity that is consistent with the record in marine sediments, thus affirming the potential value of geomagnetic excursions as important chronological markers in Quaternary sediments.

Previous magnetostratigraphic studies of loess in central Asia discovered geomagnetic transitions and excursions (e.g., Forster and Heller 1994; Fang et al. 2002; Zan et al. 2010), which greatly contributed to the chronological evaluation of the loess stratigraphy. Nevertheless, detailed paleomagnetic records including both geomagnetic directions and paleointensity variations are still scarce in the arid central Asian (ACA) region. On the other hand, the loess deposits in this area urgently need an improvement of its chronostratigraphy as there are still strong discrepancies in the ages mainly derived from radioactive dating (e.g., Feng et al. 2011; E et al. 2012; Song et al. 2012; Yang et al. 2014). In this study, we report a systematic paleomagnetic investigation of a loess section (BYH section) at the northern foot of the Tianshan Mountains in eastern ACA. Both paleomagnetic polarity and intensity variation were assessed in order to evaluate the record of geomagnetic excursions and to predict the possible applicability of short geomagnetic excursions for dating such sections in this region.

Sampling and measurements

The Tianshan Mountains are distributed in the eastern part of the ACA, separating the Tarim Basin to the south and Junggar Basin to the south. The uplift of Tianshan Mountains was affected by the deformation of the India–Asia collision zone (Sun et al. 2004), shaping the geomorphology in the arid central Asia, and meanwhile changed the atmospheric circulations affecting the local climate. Loess is widely distributed in the piedmont of the Tianshan Mountains (Ye 2001; Fang et al. 2002; Li et al. 2015a). In the northern piedmont of the Tianshan, the dusts mainly from the Saryesik-Atyrau Desert to the west and Gurbantunggut to the north formed huge loess/loessic belts with the assistance of prevailing winds (Li et al. 2015b). The BYH loess section (44.04°N, 87.80°E) is located in the northern piedmont of the Boluokenu Mountains, which belongs to the Tianshan Mountains system (Fig. 1a). The section with a thickness of 31 m was explored by a local brickyard and formed by four segments consisting of three loess–paleosol horizons (Fig. 1b). The first layer (0–1.8 m) comprises the loessic loam and weakly paleosols, which was considered to be formed during the Holocene. The loess horizon, ranging from 1.8 to 19.3 m, is characterized by uniform silt and relatively hard textures. Just beneath the loess layer, the paleosols exhibit melanocratic color with weak cementation horizon and is intercalated by two loess layers. The sampling was conducted in the well-dug trenches in the four segments of the BYH section, and oriented bulk samples were obtained at mainly 10-cm interval from the top to bottom of the loess trenches with the aid of a geological compass. After air-drying, bulk samples were then cut into 8 cm^3 cube specimens for further measurements in the laboratory.

Magnetic susceptibilities at low field of 200 A/m with both low (0.976 kHz) and high (3.904 kHz) frequencies were measured with an AGICO MFK1-FA Kappabridge. Then, percentage frequency-dependent susceptibility (χ_{fd}) was calculated by the formula: $\chi_{fd}\% = (\chi_{lf} - \chi_{hf})/\chi_{lf} \times 100\%$. Measurement of temperature-dependent magnetic susceptibility (κ-T) was taken in air condition from −192

to 700 °C using the KLY-3 Kappabridge equipped with a CS-3 and CSL device. Measurement of the AMS for all samples was taken using the same Kappabridge with magnetic susceptibility with an automated sample handling system, in which each sample was rotated through three orthogonal planes. Natural remanent magnetization (NRM) of the specimens was determined on a 2G Enterprises Model 755 U-channel cryogenic after progressive thermal demagnetization (THD) from 20 to 700 °C at 25–50 °C intervals, using a MMTD80 thermal demagnetizer. Anhysteretic remanent magnetization (ARM), expressed by anhysteretic susceptibility (χ_{ARM}), was imparted by the same instrument as for NRM measurements at a peak alternating field (AF) of 100 mT and a DC bias field of 50 μT. Isothermal remanent magnetization (IRM) was gained in stepwise pulse fields using a MMPM9 pulse magnetizer and measured using a Molspin spinner magnetometer. Hysteresis loops with relevant parameters were determined using an alternating gradient field magnetometer Micromag 2900 with a maximum field of 0.8 T. All magnetic measurements were taken at the Paleomagnetic Laboratory, Tübingen University. The accelerator mass spectrometry ^{14}C (indicated as AMS^{14}C in Fig. 1b) dating of organic matters was performed in the chronology laboratory of Lanzhou University and calibrated using the program CALIB5.01 with INTCALO4 terrestrial radiocarbon age calibration (Baillie and Reimer 2004).

Results

Magnetic mineralogy

Figure 1a–c shows the κ–T curves of representative samples from different layers in the BYH section. There is a fast decline around 580 °C in the heating curves, indicating that magnetite is the dominant magnetic mineral. The decay at c.300–450 °C along with the increase before 300 °C is noticeable in the heating curves, but both absent in the cooling curves. The lower susceptibility values after the heating–cooling run indicate the presence of maghemite (e.g., Oches and Banerjee 1996; Deng et al. 2001; Liu et al. 2005) in a single-domain or small pseudo-single-domain state, which can be easily destroyed at temperatures above c.a. 450 °C. Measurements of magnetic susceptibility under low temperature are illustrated in Fig. 1a–c with green lines. The Verwey transition (Verwey 1939) at about 120 K can be found in the low-temperature susceptibility curves, again revealing the dominance of magnetite in the typical samples. The maximum-type shape slightly above the Verwey transition indicates the isotropic point of magnetocrystalline anisotropy of magnetite (Syono 1965). Hysteresis loops have been widely used for characterizing magnetic phases and their domain state (Thompson and Oldfield 1986; Dunlop and Özdemir 1997; Evans and Heller 2003). The results from the BYH section (Fig. 2d–f) demonstrate similar magnetic properties as κ–T curves. The loops are basically closed and saturated below c. 0.3 T (with an obvious linear paramagnetic trend beyond 0.3 T), yielding a relatively low coercivity (Bc) of maximum 13.5 mT and remanence coercivities (Bcr) between 49 and 57 mT. Accordingly, the κ–T curves and hysteresis loops indicate that the magnetic properties of the BYH section are largely controlled by a ferrimagnetic phase (magnetite and maghemite).

The ratios of Mrs/Ms (saturation remanence normalized by saturation magnetization) and Bcr/Bc are two important parameters deduced from hysteresis properties and are usually analyzed in the Day plot (Day et al. 1977). The Day plot shows that the magnetic grains in the typical samples (Fig. 3a) generally exhibit the pseudo-single-domain (PSD) state. Loess samples plot in a coarser domain state range than paleosol samples in the Day plot. The King plot (King et al. 1982) is derived from the variation of χ_{ARM} with respect to χ and can intuitively evaluate the magnetic grains. As shown in Fig. 3b, most samples were distributed in a range between 1 and 5 μm,

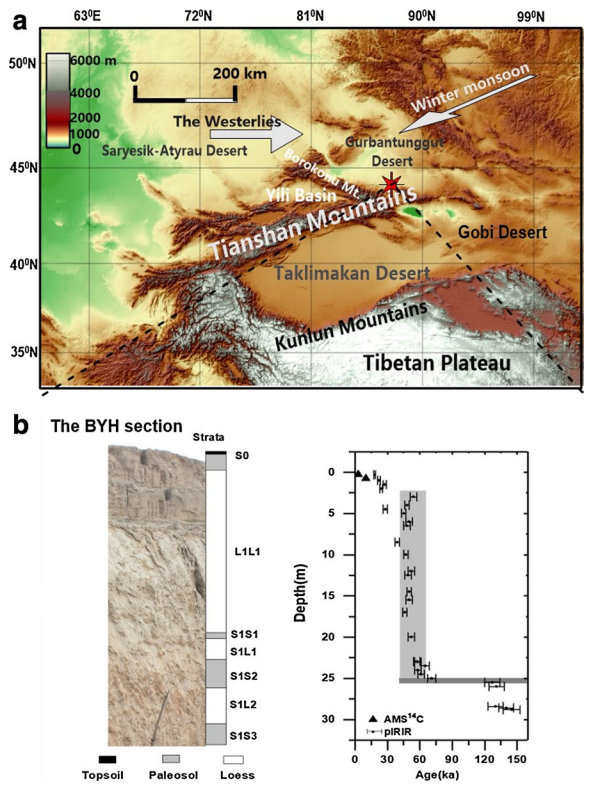

Fig. 1 **a** Schematic map showing the study area (modified from OpenTopoMap.org) and **b** sampling overview of the sampling section with main chronological constraints. (Reproduced with permission from Li et al. 2016)

indicating a relatively coarse magnetic grains in the BYH section. Similar indication were also spotted in the Dearing plot (Dearing et al. 1997), showing that all samples are generally located in the PSD + multiple domain range (Fig. 3c). And there is no significant difference between loess and paleosol samples, probably resulting from low concentration of single-domain and superparamagnetic particles during weak pedogenesis.

Characterization of magnetic anisotropy

The anisotropy of low-field magnetic susceptibility (AMS) is generally applied as an efficient and precious tool for characterizing the preferred orientation of ferro(i)magnetic minerals in rocks and sediments (Hrouda 1982). There has been an increased usage of the AMS to investigate eolian deposits, especially in loess sections for the past few years (Lagroix and Banerjee 2002, 2004; Bradák 2009; Nawrocki et al. 2010; Zhang et al. 2010; Liu and Sun 2012; Ge et al. 2014). The AMS in the loess deposits was usually associated with the syn-depositional effects or the rearrangement during post-depositional alteration, although the obstacle still remains in determination of primary and secondary fabrics in the loess deposits (Lagroix and Banerjee 2004).

Figure 4 shows the AMS properties in the BYH section. The values of lineation (L) in the BYH section range from 1 to 1.04 with an average value of 1.003, which is similar to other records in the CLP (Liu and Sun 2012). Meanwhile, a relatively developed foliation was found with values (F) ranging from 1 to 1.12, whereas the degree of anisotropy (P) shows values from 1 to 1.05 for most of the samples. Previous study in the CLP has revealed that a high degree of anisotropy ($1.032 \leq P \leq 1.064$) was associated with post-depositional loess, while wind-blown deposits show lower P values ($1.002 \leq P \leq 1.032$) (Liu and Sun 2012). Thus, the P values in the BYH section indicate that most samples underwent weak post-depositional alteration. The relation of anisotropy parameters can serve as a useful method to determine the shape of magnetic ellipsoids (Liu and Sun 2012; Ge et al. 2014). As shown in Fig. 4a, b, the F–L plot illustrates that the AMS ellipsoid for most loess samples is characterized by an oblate shape, in perfect agreement with that indicated by T–P diagram (T: the shape parameter). There is a significantly positive correlation between foliation and the anisotropy degree (Fig. 4c), expressing the dominance of foliation in the anisotropy determination. Moreover, the minimum susceptibility axis (k3) is basically distributed along the vertical axis in the stereographic plot, whereas the maximum susceptibility axis (k1) is near-horizontal and the azimuth is rather scattered (Fig. 4d). This distribution pattern of the AMS directions indicates that the AMS of the BYH section is not significantly affected by post-depositional disturbance and has remained a pristine sedimentary magnetic fabric with a prevailing oblate shape. The BYH loess section with its weak pedogenesis is therefore considered as a potentially suitable material for paleomagnetic investigation.

Paleomagnetic direction and intensity determined by ChNRM record

As shown in Fig. 5, THD of all representative samples displays a rapid and prominent decline between 200 and 300 °C with a concave-down pattern at about 300 °C, suggesting the possible effect of maghemite transformation. There is just one stable component carried mainly by the ferrimagnetic fraction that can be isolated after 250 or 300 °C for most of the measured samples. The demagnetization path until c.a 600 °C represents partial unblocking temperatures of magnetite and maghemite with different coercivities, without showing a significant directional change. In some samples, the residual remanence after thermal treatment at about 600 °C behaves erratic, reflecting a weak and unstable remanence carried by likely hematite. The reversed-polarity specimens display a generally weak viscous overprint although different levels of deviations were observed in the orthogonal projection before 300 °C in most of the specimens. The stable characteristic remanent magnetization (ChRM) directions were determined by principal component analysis (Kirschvink 1980) of at least four steps in each sample using Remasoft 3.0 software developed by the AGICO company (Chadima and Hrouda 2006). Several samples with complex THD were additionally analyzed by alternating filed magnetization with peak alternating fields from 0 to 100 mT at 5–10-mT intervals. Specimens with mean angular deviation beyond 15° or showing mismatches between inclination and declination were excluded for determining the polarity pattern. A total of 302 specimens out of 313 bulk samples were accepted for paleomagnetic analysis in this study.

In the BYH section, the NRM is carried mainly by ferrimagnetic minerals, basically magnetite. As shown in Figs. 3 and 4, most samples are constrained in PSD range and characterized by a prevailing oblate shape of anisotropy, indicating limited post-depositional alteration. Figure 6a–b illustrates the variation of main concentration-dependent magnetic parameters in the form of binary plots. Low-field magnetic susceptibility (χ) shows positive correlation with SIRM and χ_{ARM}, but with different coefficients. The values of χ range from 35.38×10^{-8} to 86.33×10^{-8} m^3 kg^{-1}, and most samples are distributed around the median value. Similar traits were also displayed in SIRM and χ_{ARM}. Very high and low values of magnetic concentration exist only in four samples that have been excluded. In general, the variation ratios

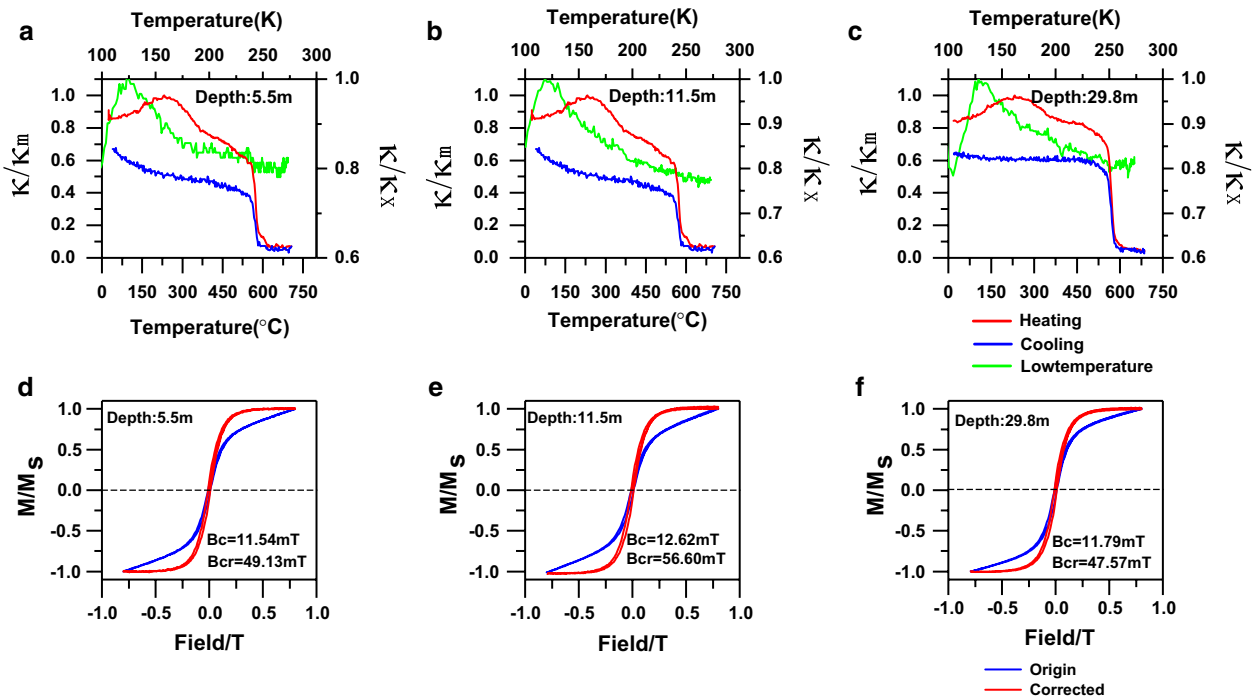

Fig. 2 **a**–**c** κ–T curves of representative samples (green line indicates the low-temperature susceptibility, while red and blues lines represent heating and cooling runs, respectively); **d**–**f** hysteresis loops of the same samples (blue lines are original data, and red lines are obtained after slope correction)

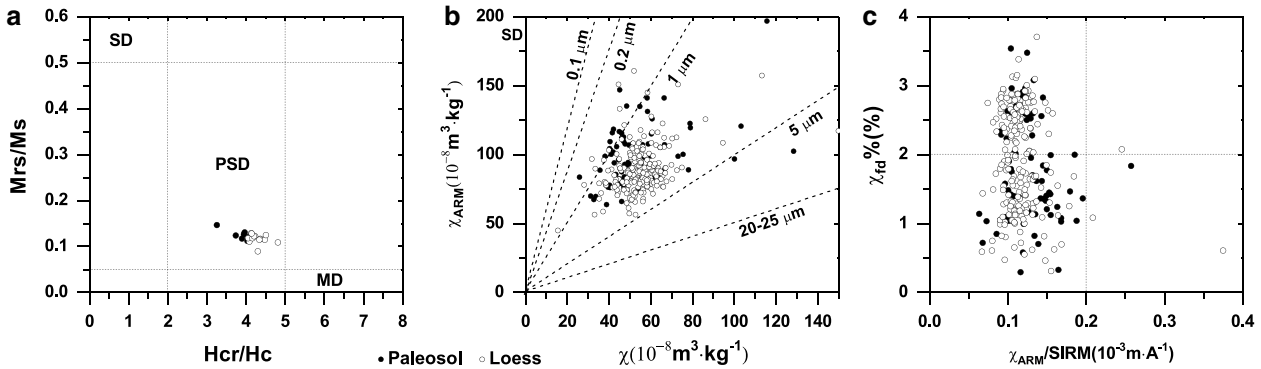

Fig. 3 **a** Representative samples in the Day plot; **b** the King plots of all samples; **c** results of all samples in the Dearing plot

between maximum and minimum values of χ, χARM and SIRM are limited in a factor of 10. As a result, rock magnetic properties of the BYH section meet the criteria (e.g., Banerjee et al. 1981; Tauxe 2005) for relative paleointensity (RPI) analysis. Since viscous remanence could be removed in most samples at 300 °C, this study chooses the NRM after THD at 300 °C ($NRM_{300\,°C}$) as the numerator. In fact, the $NRM_{300\,°C}$ has commonly been used as a suitable numerator for RPI analysis in the Chinese loess (Zhu et al. 1994; Zheng et al. 1995; Wang et al. 2014). The main concentration-dependent magnetic parameters, including mass-specific magnetic susceptibility (χ), anhysteretic remanent magnetization (ARM), and saturation isothermal remanent magnetization (SIRM), were selected to obtain normalized remanences. As shown in Fig. 6c–e, there are similar patterns in both variation and amplitude among the three RPI curves. Therefore, we tentatively combined these normalized remanences to make further analysis with five-point smoothing as shown in Fig. 6f. It is worth noting that there is an

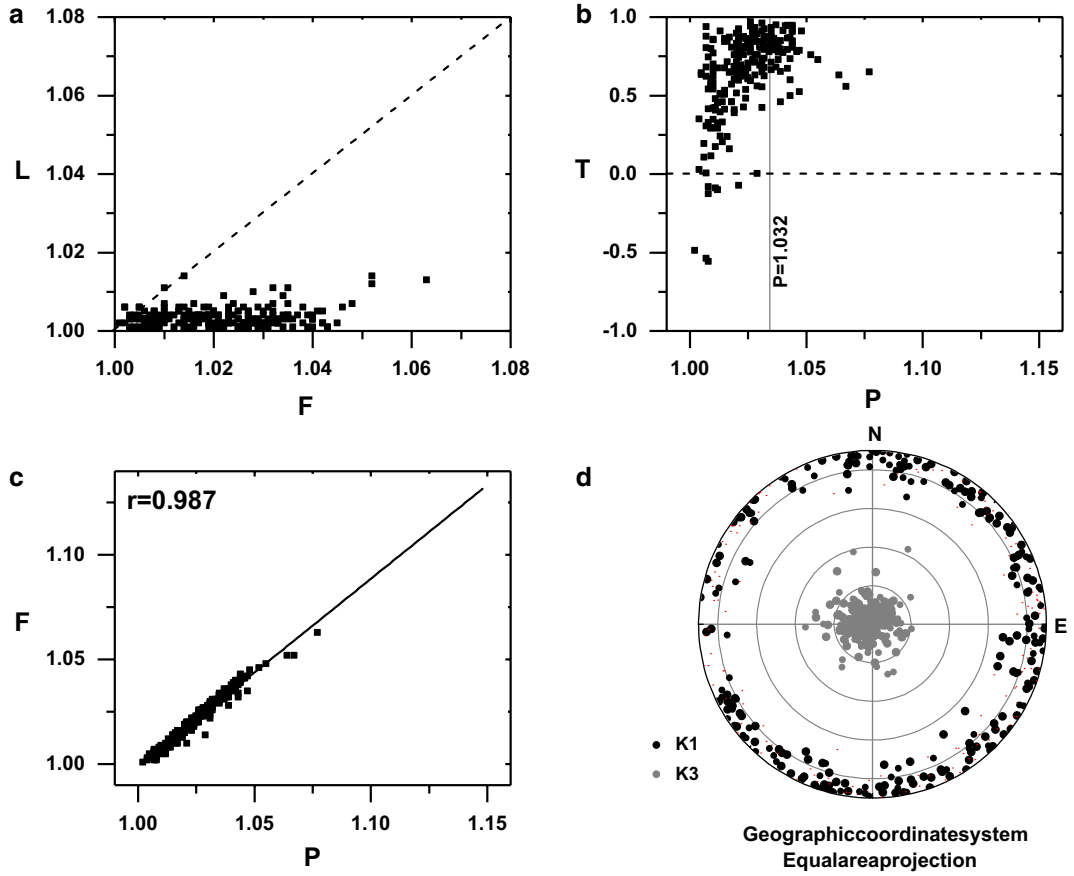

Fig. 4 **a**–**c** Bivariate relations of typical AMS parameters (*L* lineation, *F* foliation, *P* anisotropy degree); and **d** equal-area projection of AMS principal axes for all samples (black and gray circles represent k1 and k3 axes, respectively)

obvious broad peak between about 10–15 m centering at about 13 m in the stacked RPI of the BYH section. Moreover, three prominent intensity lows were located in the stratigraphic intervals centering at about 10, 17.5, 20 and 30 m.

Discussion

Remanence with less disturbance by pedogenesis

Although paleomagnetic studies have provided pivotal insights into chronological constraints for the loess–paleosol sequences, there are still uncertainties in the geomagnetic records at the millennial–centennial timescale among the loess sections mainly in the Chinese Loess Plateau (Yang et al. 2012). The first debate about the reliability of paleomagnetic signals focused on the phase discrepancy of B–M boundary between marine and loess records (Zhou and Shackleton 1999; Wang et al. 2014). In terms of this, there is a hypothesis emphasizing the timing differences of paleoclimate records in terrestrial loess with respect to the marine sediments (Zhu et al. 1998). On the other hand, Zhou et al. (1990) and Spassov et al. (2003) highlighted the effect of post-depositional alteration caused by pedogenic processes on the natural remanence based on the comparison of the B–M boundary recorded in loess and other sediments. Such lock-in phenomenon has also been observed in the study of short-lived excursions in the Chinese loess, characterized by a progressively southeastward increase in lock-in depth of the LGE (Sun et al. 2013) and the absence of paleomagnetic records of the BGE in loess sections located in the eastern part of the Loess Plateau divided by the Liupan Mountains. Zhu et al. (1998) further pointed out that the loess sections in the western Loess Plateau are able to potentially record the short-lived magnetic excursions due to a high sedimentation rate with less post-depositional disturbances.

The loess–paleosol sequences in the arid Central Asia underwent similar or even less post-depositional influence than those in the northwestern Loess Plateau, characterized by a high accumulation rate and extremely low

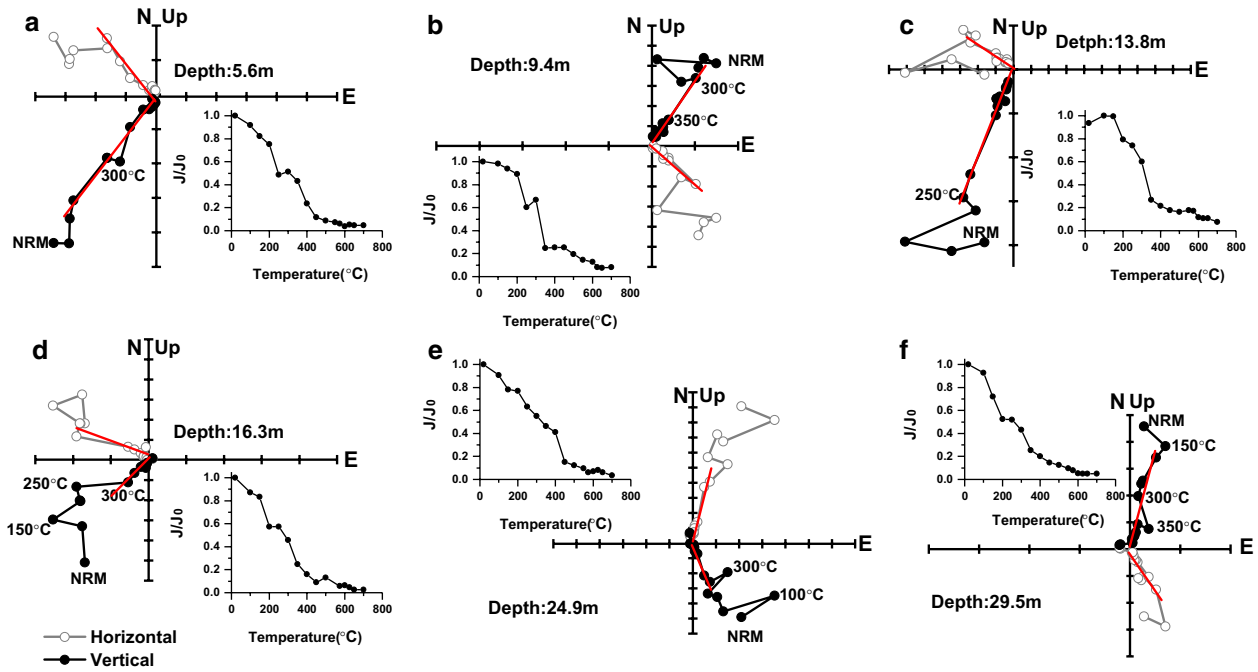

Fig. 5 Orthogonal vector projections obtained from THD of typical samples (modified from Li 2016). **a** Typical sample at the depth of 5.6 m, **b** typical sample at the depth of 9.4 m, **c** typical sample at the depth of 13.8 m, **d** typical sample at the depth of 16.3 m, **e** typical sample at the depth of 24.9 m, and **f** typical sample at the depth of 29.5 m in the BYH section. Red lines indicate the stable component isolated by thermal demagnetization

pedogenesis. It is noteworthy that the content of ultrafine magnetic particles in the BYH section is low according to values of frequency-dependent susceptibility of no more than 4% (Fig. 3c), indicating a limited contribution of pedogenesis. Meanwhile, a clear correlation between the intensities of AF demagnetization of NRM and acquisition of anhysteretic remanence at the same step was observed from 10 to 60 mT, indicating a detrital origin of the remanence carriers with relatively low coercivity (Fig. 7a). A viscous contribution could be easily erased up to 10 mT during AF demagnetization (Fig. 7b). In order to further determine the possible viscous remanences, a typical sample was selected and subjected to AF demagnetization at peak field of 150 mT. The result shows that the remanence reduced to approximately 10% of the NRM, indicating the remanences carried by soft magnetic component have been erased during the AF demagnetization. Then the sample was placed toward defined orientation in an unshielded room. The remanence show very slight variation after two mouths, and only 0.16% of the NRM was reduced during this period, suggesting a limited contribution of magnetic remanences from unstable components. Therefore, the BYH loess section likely incorporates even less post-depositional problems than the sections located in the western part of the Loess Plateau and seems suitable to document geomagnetic excursions.

Geomagnetic excursions in the BYH section

The ChRM directions of most of the samples show a normal polarity direction as illustrated in Fig. 8. The optically stimulated luminescence (OSL) ages obtained in key layers indicate that the BYH section was mainly formed in the late Quaternary within the Brunhes geomagnetic epoch (Fig. 8). A geomagnetic excursion revealed by seven specimens with fully reversed polarity along with certain samples with shallow inclinations is observed in the lower interval of the BYH section. Meanwhile, a relatively low intensity was found at c.29 m in the BYH section, corresponding to the directional anomalies in this segment. Chronologically, this paleomagnetic anomaly is probably associated with the BGE that has been globally defined at about 120 ka (Singer 2014). Besides, it can be easily detected that consecutive specimens at about 9.5 m along with relative paleointensity lows document a reversed polarity, but one of these anomalies shows shallow inclination. The OSL dating based on both quartz and feldspar (Li et al. 2016) confines the base of the anomalies with a minimum age of c. 44 ka and a maximum age of c. 47 ka, corresponding to the age of the LGE

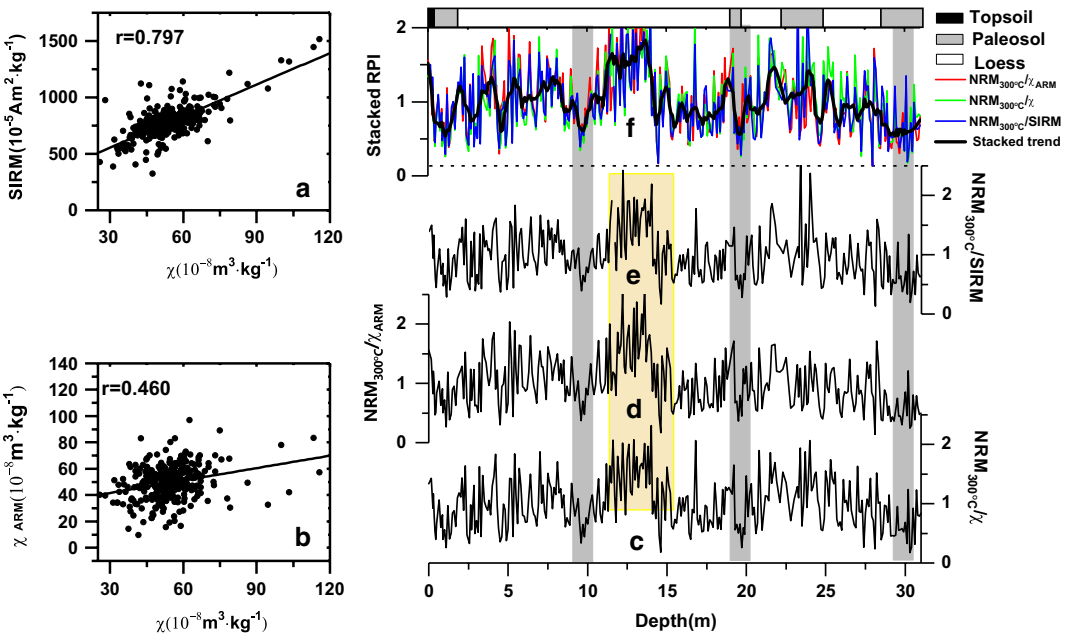

Fig. 6 Relative paleointensity (RPI) curves related to three magnetic concentration parameters. **a**, **b** Binary analysis of magnetic concentration parameters used in the RPI acquisition. **c**–**e** RPI curves obtained with different normalizers. **f** Stacked RPI in the BYH section. Gray bars highlight the RPI lows

(Sun et al. 2013; Singer 2014; Lund et al. 2017). One specimen located at 19.3 m also exhibits a reversed polarity, and a depression of geomagnetic directions was found in the neighboring positions of this anomaly in agreement with a decline in relative paleointensity. Thus, this record may not represent 'noise' record and we tentatively argue that it may possibly match with the Norwegian–Greenland Sea excursion (Laj and Channell 2007; Singer 2014) in consideration of the sampling resolution.

The BGE and LGE are two important geomagnetic markers in the Brunhes epoch and have been widely revealed in the loess–paleosol sequences via paleomagnetic (Zheng et al. 1995; Zhu et al. 1994, 1999, 2006; Fang et al. 1997; Sun et al. 2013) and cosmogenic nuclide (^{10}Be) methods (Zhou et al. 2010) since the seminal work in the 1980s (Liu 1985). In spite of the wide report in the CLP, the complete BGE record was first revealed in the Xining loess section (Fig. 9a), western part of the CLP. The BGE with duration of c.5.3 ka in the Xining section, accompanied by paleointensity lows, exhibits three evident polarity reveals intervened by two transient normal polarity zones. In addition to Xining section, the BGE was again disclosed in the Jiuzhoutai section in more detail, characterized by two short reversed intervals separated by one abrupt normal interval (Fang et al. 1997) (Fig. 9b). Our study (Fig. 9c) yields a quadruple feature of polarity swings in the bottom of the section, similar to the Xining loess record, although samples with reversed inclination are less than the two records above. The lower intensity cross the BGE region in the BYH section could be compared with the record in the Xining section (Fig. 9d, e). In terms of stratigraphy, the BGE is found in the upside of the third paleosol horizon, consistent with the upper part of Sl-c in the CLP record and loess core in the northern piedmont of Kunlun Mountains (Zan et al. 2010). The latitude and longitude of the VGPs (virtual geomagnetic poles) for the interval between 29.2 and 30.4 m are varying from 69.8°S to 65.6°N and from 9.3°E to 175.7°W, respectively. Compared to Jiuzhoutai section, the VGPs tend to be at lower latitudes (Fig. 9f). According to the present-day geomagnetic field record in the South Atlantic Anomaly region (Tarduno et al. 2014), it is possible that a given excursion might be displayed uniquely in different areas of the world and this could account for the different appearances of the BGE records. In most loess deposits in the ACA, buried paleosols were not always enhanced in magnetic concentration (e.g., Li et al. 2015a). Diagenesis under different redox conditions during the deposition could possibly affect the record of the BGE (Tarduno and Wilkison 1996), resulting in the enhancement of regional signals of the BGE. Considering the specific environment in the ACA, caution is still needed for detailed clarification of the BGE in the BYH section and further attempts are necessary to confirm the fidelity of the BGE in this area.

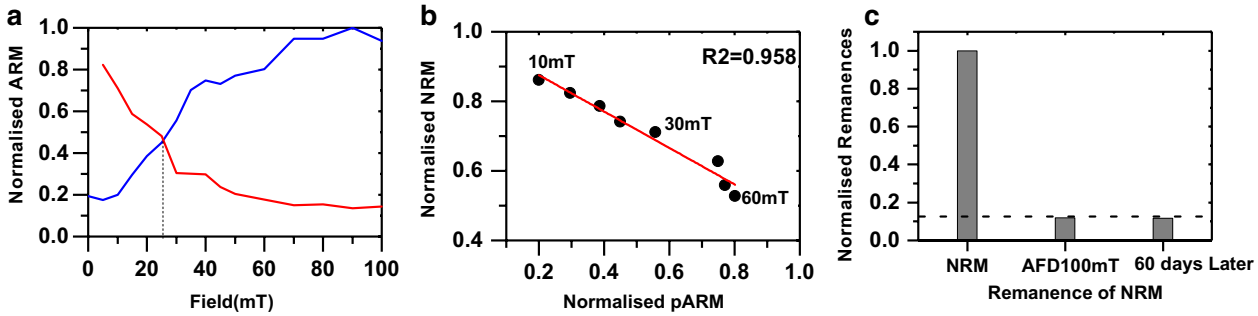

Fig. 7 **a** Alternating filed demagnetization (AFD) of normalized NRM (red curve) and acquired pARM (blue curve). **b** Remaining NRM and acquired ARM at the same applied field. **c** AFD remanences of the NRM and the variation of remanence over time

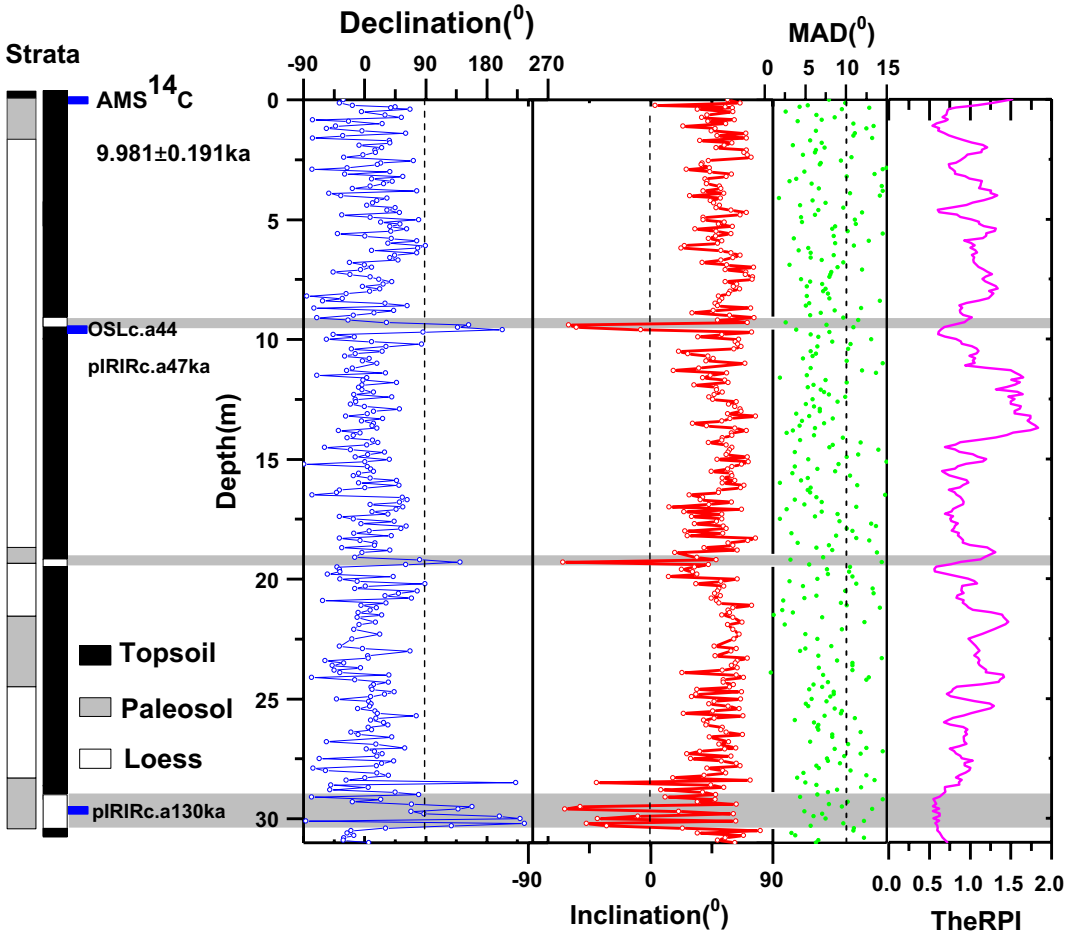

Fig. 8 Magnetostratigraphy results of the BYH loess section. The polarity zonation is defined by inclination and declination of the ChNRM derived from continuous four points with PCA. Tie point ages are shown at the left side, obtained by radiocarbon dating (AMS), and optically stimulated luminescence dating of quartz (OSL) and feldspar (pIRIR). (Reproduced with permission from Li et al. 2016)

In this study, the polarity anomalies at the segment around 9.5 m could chronologically indicate the LGE, which has been intensively discussed in the CLP (Zhu et al. 1999; Sun et al. 2013). The detailed characteristics of the LGE were first described in the Weinan section (Zhu et al. 1999), in which independence of Mono Lake excursion related to the LGE was also proved. The LGE is characterized by gradual variation of polarity reversals

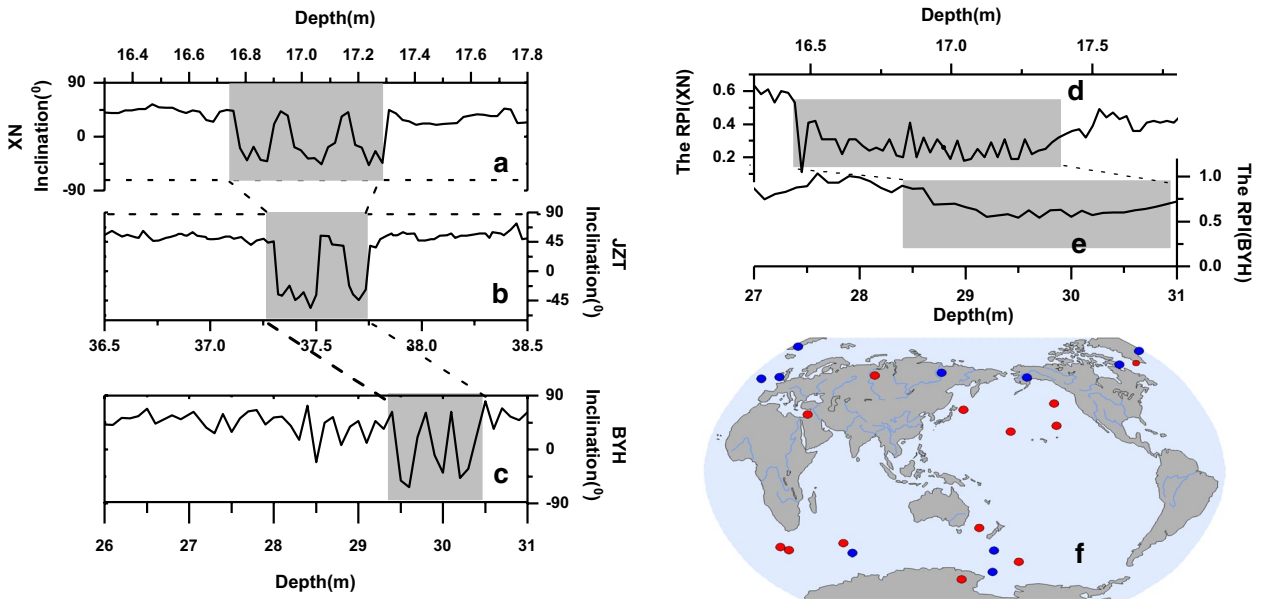

Fig. 9 Comparison of inclination record in the BYH section (**c**) with Xining (**a**) (XN, Zhu et al.1994) and Jiuzhoutai (**b**) (JZT, Fang et al. 1997) sections. The RPI record comparison between the Xining section (**d**) and the BYH section (**e**) (Zhu et al. 1994). **f** Virtual geomagnetic poles (VGPs) for the depth interval (9.1–9.9 m and 29.2–30.4 m) that contains the BGE (red) and LGE (blue), respectively, in the BYH section

in the initiation and abrupt shifting in the end in the latest publication based on a full-vector assessment (Lund et al. 2017). In the CLP, the VGPs of the LGE show two obvious polarity reversals (VGPs >45°) separated by backward trends in Weinan section and abrupt polarity reversals in Gulang section. Our results revealed similar structure with the LGE in Gulang section, and the VGPs of this interval display unantipodal distribution. The VGP of one reversed sample is located in the range that covers the VGP paths in the Gulang loess. Moreover, there is a similar chronology estimation of the LGE record between the BYH and Gulang loess. As illustrated in Sun et al. (2013), pedogenic alterations and sedimentation rates deeply affect the timing and lock-in depth in loess. The BYH section is located in the southern margin of the Gurbantunggut Desert, similar to the Gulang section that is situated in the southern margin of the Badain Jaran Desert. The higher sedimentary rate along with limited pedogenesis may possibly facilitate the record of LGE in the BYH section.

Another aspect worth mentioning is the RPI record, which contributes to a more comprehensive knowledge of historic geomagnetic behavior (Roberts et al. 1997). Along with the increasing study of the RPI, it has been noticed that the RPIs encoded in different lithologies exhibit accordant patterns. This consistency among global RPI records gives rise to several global and regional master curves of the RPI, providing a powerful tool for stratigraphic and chronological correlation in sediments. It has been widely evidenced that the main reversal or excursion correlates usually arise together with the RPI lows. Although the RPIs were introduced in the study of geomagnetic excursion in loess, the recovery of continuous RPI via paleomagnetic measurements has proved to be complex due to the post-depositional alteration during strong pedogenesis (Pan et al. 2002; Yang et al. 2007, 2012). Recently, based on the cosmogenic ^{10}Be concentration, the RPI curves have been reconstructed in typical loess sections in the CLP (Zhou et al. 2010), offering a continuous RPIs in the CLP since last interglacial. Figure 10 shows the comparison of our record with certain global and regional RPI stacks. This comparison coincides with the chronological frame from the OSL dating in several key points. There is an overall good accordance with other RPI stacks from the CLP (Zhou et al. 2010), the Northern Atlantic (e.g., Laj et al. 2000) and global marine stacks (e.g., Guyodo and Valet 1996; Channell et al. 2009) (Fig. 10), in spite of several discrepancies from the uppermost part in the studied loess section, characterized by a trend of gradually decreasing RPI. It is noteworthy that high values of the RPI were found for the interval between 11 and 14 m, corresponding to the variations of other RPI stacks at an age around 50 ka. There are also relatively low intensity zones in the RPI record of the BYH section at about 9.5, 20 and 29.5 m, which correlates well with the other four RPI stacks shown in Fig. 10, at ages centered about 41, 63 and 120 ka. This comparison not only consolidates the consistent global response

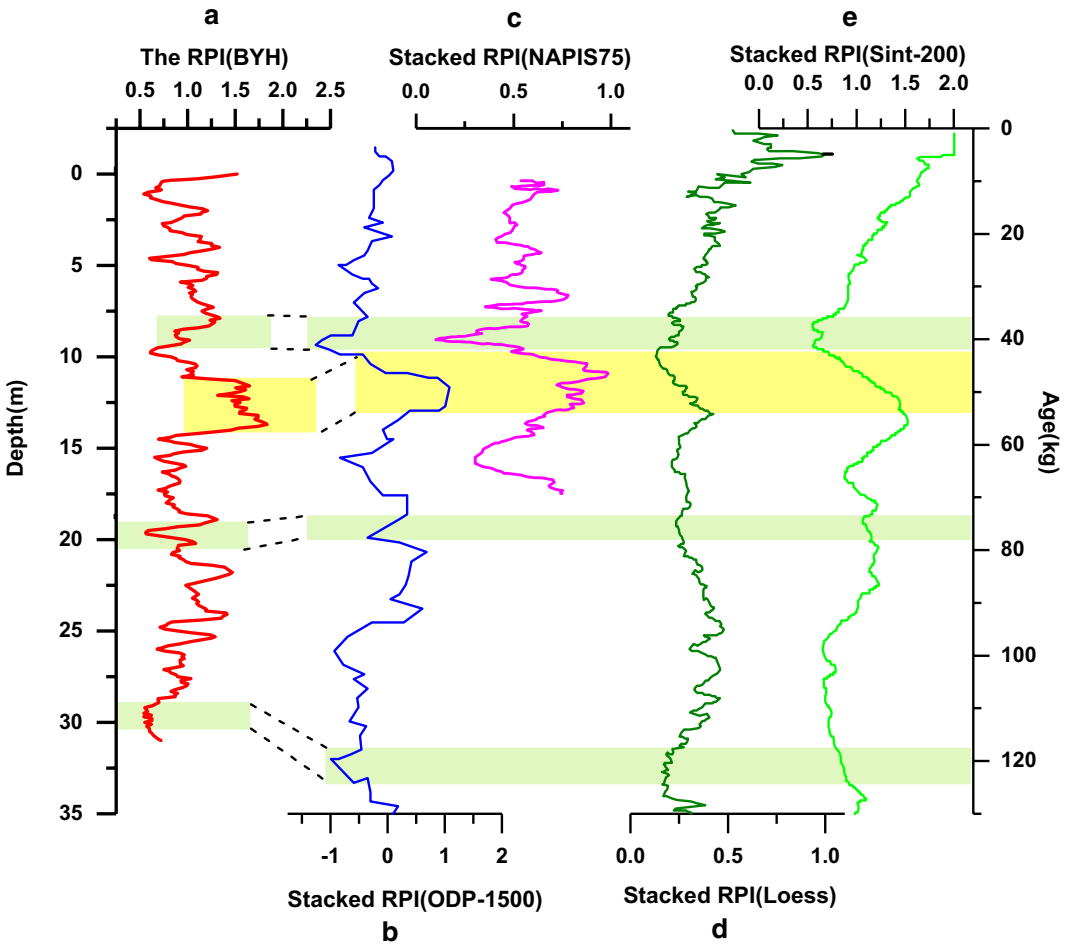

Fig. 10 Comparison of the **a** RPI record in the BYH section with **b** PISO-1500 stack (Channell et al. 2009), **c** NAPIS-75 stack (Laj et al. 2000), **d** the RPI stacks based on cosmic nuclides in the CLP (Zhou et al. 2010) and **e** the Sint-200 stack (Guyodo and Valet 1996)

to geomagnetic intensity variation, but further ascertains the possibility of the BGE and LGE record in the BYH section.

Conclusions

This study provides a paleomagnetic record, including directions and relative paleointensity, in a loess section from the northern piedmont of the Tianshan Mountain, eastern ACA. The results show that ferrimagnetic minerals dominate magnetic properties of the BYH section and serve as the main carrier for magnetic remanences. The magnetic domain state in this section is generally confined within pseudo-single-domain state, indicating that magnetic minerals remained originally depositional traits and underwent limited post-depositional alteration due to weak pedogenesis. There are three directional anomalies along with decreased intensities, two of which may chronologically be correlated to the Laschamp and Blake events, respectively. In this study, the possible Laschamp and Blake excursions were located in the loess horizon and third paleosol interval, respectively, generally corresponding to stratigraphic record of these excursions in the Chinese Loess Plateau. The Laschamp excursion shows an abrupt polarity reversal, while the Blake excursion is characterized by a quadruple structure, similar to other record in loess. The possibility of existence of the two excursions is further supported by relative paleointensity records, which indicate intensity lows in the excursion intervals. Moreover, the relative paleointensity of the BYH section may probably reflect the geomagnetic variations since last interglacial, correlated well with other global and regional RPI records.

In general, this study indicates the potential of geomagnetic excursions in the ACA loess and thus may provide an alternative tool for chronological evaluation and stratigraphic correlation in the ACA. Nevertheless, uncertainties are still remaining in the paleomagnetic record in this study, possibly resulting from the sampling

resolution and possible influence of detrital inputs from intermittent source expansion. Furthermore, diagenesis under different redox conditions during the deposition may also affect the record of the excursions in this section. The next step will be aimed at more detailed record and further confirmation of the excursions in the ACA. Multifarious methods including cosmogenic radionuclide and advanced dating techniques would benefit the refinement of the geomagnetic excursions record in the ACA.

Abbreviations

ACA: arid Central Asia; AMS: anisotropy of low-field magnetic susceptibility; IRM: isothermal remanent magnetization; ChRM: characteristic remanent magnetization; ARM: anhysteretic remanent magnetization; AF: alternating field; BGE: Blake geomagnetic excursion; LGE: Laschamp geomagnetic excursion; CLP: Chinese Loess Plateau; NRM: natural remanent magnetization; THD: thermal demagnetization; PSD: pseudo-single domain; RPI: relative paleointensity; OSL: optically stimulated luminescence.

Authors' contributions

The authors contributed to the methodology, data processing and interpretation of this manuscript. The manuscript was improved with helpful contributions from co-authors. All authors read and approved the final manuscript.

Author details

[1] Guangdong Provincal Key Laboratory of Geodynamics and Geohazards, School of Earth Sciences and Engineering, Sun Yat-sen University, Guangzhou 510275, China. [2] MOE Key LABORATORY of Western China's Environmental Systems, College of Earth and Environmental Sciences, Lanzhou University, Lanzhou 730000, Gansu, China. [3] Department of Geoscience, Eberhard Karls Universität Tübingen, 72074 Tübingen, Germany.

Acknowledgements

The authors would like to thank Yanglei Wen, Beijing Normal University, Jiabo Liu, Climate Dynamics and Landscape Evolution, Helmholtz Centre Potsdam, German Research Centre for Geosciences, and Pingyuan Li, Tongji University, for their assistance in the fieldwork and pre-treatment of the samples. We are very grateful for the precious comments and suggestions from Prof. France Lagroix, Prof. John Tarduno, chief editor and two reviewers on improving this manuscript.

Competing interests

The authors declare that they have no competing interests.

Funding

This study was supported by the National Natural Science Foundation of China (Grants 41071125 and 41704069), Guangdong Province Introduced Innovative R&D Team of Geological Processes and Natural Disasters around the South China Sea (2016ZT06N331) and China Scholarship Council (CSC).

Publisher's Note

Received: 5 January 2018 Accepted: 7 March 2018
Published online: 19 March 2018

References

Baillie MGL, Reimer PJ (2004) Intcal04 terrestrial radiocarbon age calibration, 0–26 cal kyr BP. Radiocarbon 46(3):1029–1058

Banerjee S, King J, Marvin J (1981) A rapid method for magnetic granulometry with applications to environmental studies. Geophys Res Lett 8(4):333–336

Bonhommet N, Babkine J (1967) Sur la presence d'aimentation inverse dans la Chaine des Puys. C.R. Hebs. Comptes Rendus de l'Académie des Sciences Paris B264:92–94

Bradák B (2009) Application of anisotropy of magnetic susceptibility (AMS) for the determination of paleo-wind directions and paleo-environment during the accumulation period of Bag Tephra, Hungary. Quat Int 198(1–2):77–84

Cassata WS, Singer BS, Cassidy J (2008) Laschamp and Mono Lake geomagnetic excursions recorded in New Zealand. Earth Planet Sci Lett 268:76–88

Chadima M, Hrouda F (2006) Remasoft 3.0-a user-friendly paleomagnetic data browser and analyzer. Trav Géophys XXVII:20–21

Channell JET (2006) Late Brunhes polarity excursions (Mono Lake, Laschamp, Iceland Basin and Pringle Falls) recorded at ODP site 919 (Irminger basin). Earth Planet Sci Lett 244(1):378–393

Channell J, Xuan C, Hodell D (2009) Stacking paleointensity and oxygen isotope data for the last 1.5 Myr (PISO-1500). Earth Planet Sci Lett 283:14–23

Day R, Fuller M, Schmidt V (1977) Hysteresis properties of titanomagnetites: grain size and composition dependence. Phys Earth Planet Inter 13:260–267

Dearing J, Bird P, Dann R, Benjamin S (1997) Secondary ferrimagnetic minerals in welsh soils: a comparison of mineral magnetic detection methods and implications for mineral formation. Geophys J Int 130(3):727–736

Deng C, Zhu R, Jackson M, Verosub K, Singer M (2001) Variability of the temperature-dependent susceptibility of the Holocene eolian deposits in the Chinese loess plateau: a pedogenesis indicator. Phys Chem Earth Part A 26(11–12):873–878

Denham C (1976) Blake polarity episode in two cores from the Greater Antilles Outer Ridge. Earth Planet Sci Lett 29(2):422–434

Dunlop D, Özdemir Ö (1997) Rock magnetism: fundamentals and frontiers. Cambridge University Press, Cambridge

E ChongYi, Lai Z, Sun Y, Hou G, Yu L, Wu C (2012) A luminescence dating study of loess deposits from the Yili river basin in Western China. Quat Geochronol 10(10):50–55

Evans M, Heller F (2003) Environmental magnetism. Academic Press, New York

Fang X, Li J, Voo R, Niocaill C, Dai X, Kemp R, Derbyshire E, Cao J, Wang J, Wang G (1997) A record of the Blake event during the last interglacial paleosol in the western loess plateau of China. Earth Planet Sci Lett 146(1–2):73–82

Fang X, Shi Z, Yang S, Yan M, Jijun LI, Jiang P (2002) Loess in the Tian Shan and its implications for the development of the Gurbantunggut Desert and drying of northern Xinjiang. Chin Sci Bull 47(16):1381–1387

Feng Z, Ran M, Yang Q, Zhai X, Wang W, Zhang X, Huang C (2011) Stratigraphies and chronologies of late quaternary loess–paleosol sequences in the core area of the central Asian arid zone. Quat Int 240(1):156–166

Forster T, Heller F (1994) Paleomagnetism of loess deposits from the Tajik depression (Central Asia). Earth Planet Sci Lett 128:501–512

Ge J, Guo Z, Zhao D, Zhang Y, Wang T, Yi L, Deng C (2014) Spatial variations in paleowind direction during the last glacial period in north China reconstructed from variations in the anisotropy of magnetic susceptibility of loess deposits. Tectonophysics 629(629):353–361

Guillou H, Scao V, Nomade S (2016) Blake excursion at vulcano (Aeolian Islands, Italy): revised k-ar and 40 ar/39 ar ages. Quat Geochronol 35:77–87

Guyodo Y, Valet J (1996) Relative variations in geomagnetic intensity from sedimentary records: the past 200.000 years. Earth Planet Sci Lett 143(1–4):23–36

Hrouda F (1982) Magnetic anisotropy of rocks and its application in geology and geophysics. Surv Geophys 5(1):37–82

King J, Banerjee SK, Marvin J, Özdemir Özden (1982) A comparison of different magnetic methods for determining the relative grain size of magnetite in natural materials: some results from lake sediments. Earth Planet Sci Lett 59(2):404–419

Kirschvink J (1980) The least-squares line and plane and the analyses of paleomagnetic data. Geophys J R Astr Soc 62:699–718

Lagroix F, Banerjee SK (2002) Paleowind directions from the magnetic fabric of loess profiles in central Alaska. Earth Planet Sci Lett 195(1):99–112

Lagroix F, Banerjee SK (2004) Cryptic post-depositional reworking in aeolian sediments revealed by the anisotropy of magnetic susceptibility. Earth Planet Sci Lett 224(3):453–459

Laj C, Channell JET (2007) Geomagnetic excursions. In: Kono M (ed) Treatise on geophysics. Geomagnetism, vol 5. Elsevier, Amsterdam, pp 373–416

Laj C, Kissel C, Mazaud A, Beer J (2000) North Atlantic palaeointensity stack since 75 ka (NAPIS-75) and the duration of the Laschamp event. Philos Trans R Soc Lond Ser A 358(1768):1009–1025

Lascu I, Feinberg J, Dorale J, Cheng H, Edwards R (2016) Age of the Laschamp excursion determined by u-th dating of a speleothem geomagnetic record from North America. Geology 44(G37490):1
Li G (2016) Magnetostratigraphy of loess deposits in the north of Xinjiang. Lanzhou University, Lanzhou, China
Li G, Xia D, Jia J, Zhao S, Gao F, Wang Y et al (2015a) Magnetic properties derived from a loess section at the northern piedmont of Tianshan mountains, Xinjiang, China, and their paleoenvironmental significance. Geophys J Int 203(2):828–839
Li Y, Song Y, Yan L, Chen T, An Z (2015b) Timing and spatial distribution of loess in Xinjiang, NW China. PLoS ONE. https://doi.org/10.1371/journal.pone.0125492
Li G, Rao Z, Duan Y, Xia D, Wang L, Madsen D, Jia J, Wei H, Qiang M, Chen J, Chen F (2016) Paleoenvironmental changes recorded in a luminescence dated loess/paleosol sequence from the Tianshan Mountains, arid central Asia, since the penultimate glaciation. Earth Planet Sci Lett 448:1–12
Liu TS (1985) Loess and the environment. Science Press, Beijing
Liu W, Sun J (2012) High-resolution anisotropy of magnetic susceptibility record in the central Chinese Loess Plateau and its paleoenvironment implications. Sci China Ser D Earth Sci 55(3):488–494
Liu Q, Deng C, Yu Y, JosÉ T, Jackson M, Banerjee S, Zhu R (2005) Temperature dependence of magnetic susceptibility: implications for pedogenesis of Chinese loess/palaeosols. Geophys J Int 161(1):102–112
Lund S, Schwartz M, Keigwin L, Johnson T (2005) Deep-sea sediment records of the Laschamp geomagnetic field excursion (~41,000 calendar years before present). J Geophys Res B Solid Earth 110(B4):B04101
Lund S, Benson L, Negrini R, Liddicoat J, Mensing S (2017) A full-vector paleomagnetic secular variation record (PSV) from pyramid lake (Nevada) from 47–17 ka: evidence for the successive mono lake and Laschamp excursions. Earth Planet Sci Lett 458:120–129
Nawrocki J, Polechoǹska O, Boguckij A, Łanczont Maria (2010) Palaeowind directions recorded in the youngest loess in Poland and western Ukraine as derived from anisotropy of magnetic susceptibility measurements. Boreas 35(2):266–271
Nowaczyk N, Arz H, Frank U, Kind J, Plessen B (2012) Dynamics of the Laschamp geomagnetic excursion from Black Sea sediments. Earth Planet Sci Lett s 351–352(11):54–69
Oches EA, Banerjee SK (1996) Rock-magnetic proxies of climate change from loess–paleosol sediments of the Czech Republic. Stud Geophys Geod 40(3):287–300
Osete M, Martín-Chivelet J, Rossi C, Edwards R, Egli R, Muñoz-García M, Wang X, Pavón-Carrascoa J, Hellerh F (2012) The Blake geomagnetic excursion recorded in a radiometrically dated speleothem. Earth Planet Sci Lett s 353–354((s 1–4)):173–181
Pan Y, Zhu R, Liu Q, Guo B, Yue L, Wu H (2002) Geomagnetic episodes of the last 1.2 Myr recorded in Chinese loess. Geophys Res Lett 29(8):123-1–123-4
Roberts AP (2008) Geomagnetic excursions: knowns and unknowns. Geophys Res Lett 35(17):L17307
Roberts A, Winklhofer M (2004) Why are geomagnetic excursions not always recorded in sediments? Constraints from post-depositional remanent magnetization lock-in modeling. Earth Planet Sci Lett 227:345–359
Roberts AP, Lehman B, Weeks RJ, Verosub KL, Laj C (1997) Relative paleointensity of the geomagnetic field over the last 200,000 years from ODP sites 883 and 884, North Pacific Ocean. Earth Planet Sci Lett 152((s 1–4)):11–23
Singer B (2014) Quaternary geomagnetic instability time scale. Quat Geochronol 21(6):29–52
Singer B, Guillou H, Jicha B, Laj C, Kissel C, Beard B, Johnson C (2009) 40Ar/39Ar, K-Ar and 230 Th–238U dating of the Laschamp excursion: a radioisotopic tie-point for ice core and climate chronologies. Earth Planet Sci Lett 286(1):80–88
Smith J, Foster J (1969) Geomagnetic reversal in Brunhes normal polarity epoch. Science 163(163):565–567
Song Y, Li C, Zhao J, Cheng P, Zeng M (2012) A combined luminescence and radiocarbon dating study of the Ili loess, Central Asia. Quat Geochronol 10(4):2–7
Spassov S, Heller F, Evans M, Yue L, Dobeneck T (2003) A lock-in model for the complex Matuyama–Brunhes boundary record of the loess/palaeosol sequence at Lingtai (Central Chinese, Loess Plateau). Geophys J Int 155(2):350–366
Sun J, Zhu R, Bowler J (2004) Timing of the Tianshan Mountains uplift constrained by magnetostratigraphic analysis of molasse deposits. Earth Planet Sci Lett 219(3–4):239–253
Sun Y, Qiang X, Liu Q, Bloemendal J (2013) Wang, X (2013) Timing and lock-in effect of the Laschamp geomagnetic excursion in Chinese Loess. Geochem Geophys Geosyst 14(11):4952–4961
Syono Y (1965) Magnetocrystalline anisotropy and magnetostriction of Fe3O4,-Fe2TiO4, Series-with Special Application to Rock Magnetism. Jpn. J. Geophys. 4(1):71–143
Tarduno JA, Wilkison SL (1996) Non-steady state magnetic mineral reduction, chemical lock-in, and delayed remanence acquisition in pelagic sediments. Earth Planet Sci Lett 144(3–4):315–326
Tarduno J, Watkeys M, Huffman T, Cottrell R, Blackman E, Wendt A, Scribner C, Wagner C (2014) Antiquity of the south atlantic anomaly and evidence for top-down control on the geodynamo. Nat. Commun. 6:7865
Tauxe, L (2005) Lectures in Paleomagnetism, http://earthref.org/MAGIC/books
Thompson R, Oldfield F (1986) Environmental Magnetism. Allen & Unwin, London
Tucholka P, Fontugne M, Guichard F, Paterne M (1987) The Blake magnetic polarity episode in cores from the Mediterranean Sea. Earth Planet Sci Lett 86(2–4):320–326
Valet JP, Meynadier L (1993) Geomagnetic field intensity and reversals during the past four million years. Nature 366:234–238
Verwey E (1939) Electronic conduction of magnetite (Fe3O4) and its transition point at low temperatures. Nature 144:327–328
Wang X, Løvlie R, Chen Y, Yang Z, Pei J, Tang L (2014) The Matuyama–Brunhes polarity reversal in four Chinese loess records: high-fidelity recording of geomagnetic field behavior or a less than reliable chronostratigraphic marker? Quat Sci Rev 101(5):61–76
Yamazaki T, Kanamatsu T (2007) A relative paleointensity record of the geomagnetic field since 1.6 Ma from the North Pacific. Earth Planets Space 59(7):785–794. https://doi.org/10.1186/BF03352741
Yang T, Hyodo M, Yang Z, Ding L, Fu J (2007) Early and middle Matuyama geomagnetic excursions recorded in the Chinese loess–paleosol sediments. Earth Planets Space. 59(7):825–840. https://doi.org/10.1186/BF03352745
Yang T, Li H, Wu H, Yang Z, Zhang S, Masayuki H (2012) Reliability of relative paleointensity recorded in Chinese loess–paleosol sediments. Acta Geol Sin 86(5):1276–1288
Yang S, Forman SL, Song Y, Pierson J, Mazzocco J, Li X, Shi Z, Fang X (2014) Evaluating OSL-SAR protocols for dating quartz grains from the loess in Ili basin, central Asia. Quat Geochronol 20(2):78–88
Ye W (2001) The loess deposition features and paleoclimate in westerly region of Xinjiang. Ocean Press, Beijing
Zan J, Fang X, Yang S, Nie J, Li X (2010) A rock magnetic study of loess from the West Kunlun Mountains. J Geophys Res B Solid Earth 115:B10101. https://doi.org/10.1029/2009JB007184
Zhang R, Kravchinsky VA, Zhu R, Yue L (2010) Paleomonsoon route reconstruction along a w–e transect in the Chinese loess plateau using the anisotropy of magnetic susceptibility: summer monsoon model. Earth Planet Sci Lett 299(3):436–446
Zheng H, Rolph T, Shaw J, An Z (1995) A detailed palaeomagnetic record for the last interglacial period. Earth Planet Sci Lett 133(3–4):339–351
Zhou LP, Shackleton NJ (1999) Misleading positions of geomagnetic reversal boundaries in eurasian loess and implications for correlation between continental and marine sedimentary sequences. Earth Planet Sci Lett 168(1–2):117–130
Zhou L, Oldfield F, Wintle A, Robinson S, Wang J (1990) Partly pedogenic origin of magnetic variations in Chinese loess. Nature 346(6286):737–739
Zhou W, Feng X, Beck W, Jull A, An Z, Wu Z, Liu M, Chen M, Priller A, Kutschera W, Burr G, Yu H, Song S, Cheng P, Kong X (2010) Reconstruction of 130-kyr Relative Geomagnetic Intensities from 10Be in Two Chinese Loess Sections. Radiocarbon 52(1):129–147
Zhu R, Zhou L, Laj C, Mazaud A, Ding Z (1994) The Blake geomagnetic polarity episode recorded in Chinese loess. Geophys Res Lett 21(21):697–700
Zhu R, Coe R, Guo B, Anderson R, Zhao X (1998) Inconsistent palaeomagnetic recording of the Blake event in Chinese loess related to sedimentary environment. Geophys J Int 134(3):867–875
Zhu R, Pan Y, Liu Q (1999) Geomagnetic excursions recorded in Chinese loess in the last 70,000 years. Geophys Res Lett 26:505–508
Zhu R, Liu Q, Pan Y, Deng C, Zhang R, Wang X (2006) No apparent lock-in depth of the Laschamp geomagnetic excursion: evidence from the Malan loess. Sci China Ser D Earth Sci 49(9):960–967